Hydrogen-bonded complexes of acetylene and acetonitrile: A matrix isolation infrared and computational study

ARTICLE *in* JOURNAL OF MOLECULAR STRUCTURE · MARCH 2015

Impact Factor: 1.6 · DOI: 10.1016/j.molstruc.2014.11.024

3 AUTHORS:

Gopi Ragupathy
Indira Gandhi Centre for Atomic Research
10 PUBLICATIONS **8** CITATIONS
SEE PROFILE

N. Ramanathan
Indira Gandhi Centre for Atomic Research
30 PUBLICATIONS **93** CITATIONS
SEE PROFILE

Kalyansundaram Sundararajan
Indira Gandhi Centre for Atomic Research
50 PUBLICATIONS **442** CITATIONS
SEE PROFILE

Journal of Molecular Structure 1083 (2015) 364–373

Contents lists available at ScienceDirect

Journal of Molecular Structure

journal homepage: www.elsevier.com/locate/molstruc

Hydrogen-bonded complexes of acetylene and acetonitrile: A matrix isolation infrared and computational study

R. Gopi, N. Ramanathan, K. Sundararajan *

Chemistry Group, Indira Gandhi Centre for Atomic Research, Kalpakkam 603 102, India

HIGHLIGHTS

- Experimental evidence for the formation of 1:1 CH···N complex of C_2H_2—CH_3CN.
- The experimental and calculated vibrational wavenumbers agreed well with each other
- Higher 1:2 C_2H_2—$(CH_3CN)_2$ and 2:1 $(C_2H_2)_2$—CH_3CN complexes were also observed.
- The nature of interaction in the complexes was characterized by AIM and NBO analysis.

ARTICLE INFO

Article history:
Received 17 September 2014
Received in revised form 28 October 2014
Accepted 10 November 2014
Available online 15 November 2014

Keywords:
H-bonded complexes
Acetylene
Acetonitrile
Matrix isolation
Infrared
Ab initio calculations

ABSTRACT

Hydrogen-bonded complexes of acetylene (C_2H_2) and acetonitrile (CH_3CN) have been investigated using matrix isolation infrared spectroscopy and *ab initio* computations. The complexes were trapped in both solid argon and N_2 matrices. The structure of the complexes and the energies were computed at the B3LYP and MP2 levels of theory using a 6-311++G(d,p) basis set and also at B3LYP/aug-cc-pVDZ level. Our computations indicated one minimum corresponding to the 1:1 C_2H_2—CH_3CN complex, with C—H···N interaction, where C_2H_2 is the proton donor. Experimentally, we observed the 1:1 C_2H_2—CH_3CN complex in Ar and N_2 matrices, which was evidenced by the shifts in the vibrational wavenumbers of the modes involving the C_2H_2 and CH_3CN sub-molecules. Computations were also performed to study the higher complexes of C_2H_2 and CH_3CN. One minimum was found for the 1:2 C_2H_2—CH_3CN complex and two minima for the 2:1 C_2H_2—CH_3CN complexes, at all levels of theory. Experimentally we observed features corresponding to the 1:2 C_2H_2—CH_3CN complexes in an Ar and N_2 matrices. The computed vibrational wavenumbers of C_2H_2—CH_3CN complexes at B3LYP/6-311++G(d,p) level correlate well with the experimental wavenumbers. Atoms in Molecules (AIM) analysis was performed to understand the nature of interaction in the complexes. Natural Bond Orbital (NBO) analysis was performed to understand the effect of charge-transfer hyperconjugative interactions towards the stability of different C_2H_2—CH_3CN complexes.

Introduction

Studies of hydrogen-bonded complexes, both experimental and theoretical, are of considerable interest [1–14]. The conventional hydrogen bond (H-Bond) where an X—H bond interacts with Y is represented by X—H···Y. Here X is an electronegative atom and Y with its electrons is a hydrogen bond acceptor and the formation of the H-Bond results in a red-shift of the X—H stretching frequency. There are a number of experimental and theoretical studies on this subject. During the last fifteen years there has been an emphasis on the study of weak hydrogen bonds involving C—H···O, C—H···π, O—H···π and C—H···N interactions, as these serve as a driving force for many molecular phenomena and processes in chemistry, biology and material science [15]. Our interest in these weak hydrogen-bonded systems led early studies on hydrogen bonded complexes formed by CHF_3, $CHCl_3$, C_2H_4, C_6H_6 and C_6H_5N with C_2H_2 using matrix isolation infrared spectroscopy in an Ar matrix [16–19].

We have earlier found the experimental evidences for the 1:1 n–σ complex of C_2H_2 and Pyridine (C_6H_5N) in an Ar matrix. The complex is stabilized by C—H···N, where the H-bonded interaction is between the hydrogen of C_2H_2 and the lone pair of electrons on the nitrogen. *Ab initio* computations at the HF and B3LYP levels of theory using a 6-311++G(d,p) basis set were performed on the C_2H_2—NC_6H_5 complex supported the experimental observations [19].

* Corresponding author. Tel.: +91 044 27480098; fax: +91 044 27480065.
E-mail address: sundar@igcar.gov.in (K. Sundararajan).

http://dx.doi.org/10.1016/j.molstruc.2014.11.024
0022-2860/

Acetonitrile, CH_3CN has a unique properties such as high dielectric constant and remarkable miscibility with range of ionic and polar solvents [20] which makes CH_3CN as a solvent of choice for variety of organic synthesis. CH_3CN is also used as a mobile phase in HPLC and LC–MS. CH_3CN has been extensively used in synthetic organic chemistry and enormous literature on this area has been reported. Earlier, Freedman and Nixon investigated the infrared spectra of CH_3CN in solid argon matrix [21]. Later, Kim and Kim re-investigated the vibrational spectra of CH_3CN using Fourier transform infrared spectra and made precise assignments of monomers, dimers and higher mulitmers of CH_3CN [22]. Givan and Loewenschuss studied the Raman spectrum of CH_3CN using matrix isolation spectroscopy [23]. Coussan et al. studied the CH_3OH—CH_3CN complexes trapped in Ar and N_2 matrices. On photolysis, they observed both hydrogen-bonded homo and hetero aggregates of methanol in these matrices. Further, these aggregates are better formed in an Ar than in N_2 matrix [24]. Kryachko and Nguyen theoretically studied the hydrogen-bonded complexes of phenol and CH_3CN [25]. The computational results were correlated well with the experiments [26–29]. From the computations they predicted phenol and CH_3CN forms 1:1 σ and π-type complexes, where the former is more stable than the later. The π-type structure becomes more stable when one more acetonitrile molecule interacts with 1:1 phenol-acetonitrile complex. Phillips et al. studied the vibrational spectra of CH_3CN—BF_3 complexes in solid argon [30]. Later, Shimizu et al. studied the matrix effects on the vibrational spectra of the CH_3CN—BF_3 complex in solid matrices of Ar, N_2, and Xe [31].

Doo-sik Ahm and Sungyul Lee computationally studied the σ- and π-type hydrogen-bonded complexes of acetonitrile–water clusters. They found at MP2/6-31+G(d,p) level of theory the π-type complex is slightly lower in ZPE corrected energy by 0.11 kcal/mol, while the σ-type complex is of lower energy by 0.09 kcal/mol when MP2/aug-cc-pVDZ level of theory is employed [32].

Mixtures of CH_3CN and water are popular solvents and has been studied extensively both experimentally and theoretically [33–38]. Rutkowski et al. studied the formation of 1:1 complexes between acetylene and trimethylamine in liquefied krypton solvent. They observed red shift in the C—H region and blue shift in the CN stretching region in the complex. The experimental wavenumbers were correlated with MP2/6-311++G(2d,2p) level of theory [39]. Domagala and Gabrowski performed *ab initio* computations on the hydrogen-bonded complexes between hydrogen cyanide $(HCN)\cdots HF$ and acetylene $(C_2H_2)\cdots HF$ using B3LYP and MP2 levels of theory with 6-311++G(d,p) basis set. They found that π-electrons of acetylene act as a proton accepting centers and the $C_2H_2\cdots HF$ complex forms a T-shaped structure whereas in the $HCN\cdots HF$ complex, the nitrogen atom in the hydrogen cyanide molecule acts as the proton acceptor center but not π-electrons [40]. Ault et al. reported photochemical reaction of CH_3CN with $CrCl_2O_2$ and $OVCl_3$ and the product was trapped in an Ar matrix. The formation of 1:1 complex was identified using UV/Vis spectroscopy. When the matrix was irradiated with light of $\lambda > 300$ nm, new features in the infrared spectra was observed and assigned for $ONCCH_3$ complexes of CH_3CN n-oxide with $CrCl_2O$ and VCl_3, respectively. Identification of these species was supported by extensive isotopic labeling (^2H and ^{15}N), as well as by B3LYP/6-311++G(d,2p) density functional calculations [41]. Suzuki et al. studied the 1:1 hydrogen-bonded complexes of acetonitrile with BF_3 in Ar, N_2 and Xe matrices. The experimental observed shift agreed well the calculation performed at B3LYP/6-311++G(d,p) level of theory [42]. Samet et al. studied the C—H···N hydrogen-bonded complexes of pentachlorocyclopropane (PCCP) with the bases acetonitrile, ammonia, monomethyl amine and dimethyl amine isolated in argon matrices at 10 K. Both IR spectroscopy and DFT computations supported the formation of 1:1 complexes between PCCP with different bases which was evidenced from the shift in the vibrational modes of PCCP and base sub-molecule [43].

Allamandola et al. studied 16 nitriles and related compounds in Ar and H_2O matrices. The strong C≡N stretching vibrations of these compounds are probed using vibrational spectroscopy in matrices. The absorption band of these nitriles in Ar and H_2O matrices are then used to facilitate the search for these features observed by Infrared Space Observatory (ISO) [44]. Several groups studied the C—H···N interactions both by experimental and theoretical methods [45–48]. Recently, Zins and Krim studied the formation of 1:1 complex between Acetonitrile (CH_3CN) and formic acid (HCOOH) in neon matrix. The formation of the 1:1 complex is evidenced in the modes corresponding to the formic acid and acetonitrile sub-molecules. *Ab initio* computations performed at MP2/6-31++G(d,p) and MP2/aug-cc-pVTZ level of theories gave one minima for the 1:1 and 2:1 complex and two minima for the 1:2 complex. Experimentally, they also observed 2:1 and 1:2 CH_3CN—HCOOH complexes in Ne matrix. Further, they have photolysed the Ne matrix using VUV photons. The photochemical reaction induces the formation cyanomethanoic acid [49].

To best of our knowledge there is no matrix isolation infrared studies on the C_2H_2 with CH_3CN system. CH_3CN has two electron rich sites, lone pairs on nitrogen and C≡N triple bond, which can form either a σ- or π-type hydrogen bond or both. Acetylene (C_2H_2) acts as a proton donor as the hydrogen attached to the 'sp' carbon atom is sufficiently acidic. Alternatively, C_2H_2 can also play the role of a proton acceptor through its π-cloud. It is interesting to study the interaction between the C_2H_2 and CH_3CN and to see the competing ability of CH_3CN and C_2H_2 as proton donors and acceptors. The present work is carried out with an aim to explore the possibility of forming 1:1 complexes between C_2H_2 and CH_3CN in Ar and N_2 matrices and to correlate with the computational results. We also explored the formation of higher C_2H_2—CH_3CN complexes both computationally and experimentally.

Experimental and computational methods

Matrix isolation experiments were performed using a RDK-408D2 (Sumitomo Heavy Industries Ltd.) closed cycle helium compressor cooled cryostat. The cryostat was housed in a vacuum chamber where the base pressure was $<1 \times 10^{-6}$ mbar. C_2H_2 (Commercial Grade, Asiatic Oxygen Limited, India) and CH_3CN (Merck, HPLC grade 99.8%) were used as such, without further purification. Ar and N_2 (IOLAR Grade 2) is used as matrix gases, in which C_2H_2 were pre-mixed to obtain the desired matrix-to-sample ratios. The C_2H_2/matrix gas mixture and CH_3CN was then deposited using double jet nozzle onto a KBr substrate maintained at 12 K. We used typical matrix-to-sample ratios ranging from 1000:0.1 to 1000:0.2 for C_2H_2 and 1000:1 to 1000:2.5 for CH_3CN. The matrix was then deposited at a typical rate of ~3 mmol/h and a deposition typically lasted for about 60 min.

Infrared spectra of the matrix isolated samples were recorded in the range 4000–400 cm^{-1}, using a BOMEM MB 100 FTIR spectrometer, operated at a resolution of 1 cm^{-1}. The matrix was then slowly warmed to 35 K for Ar and 30 K for N_2 which was maintained at this temperature for about 15 min and then re-cooled to 12 K. Spectra of the annealed matrix were again recorded.

Theoretical calculations were performed for the C_2H_2—CH_3CN complexes using GAUSSIAN 94W suite of programs package running on a Pentium 4 machine with 3.0 GHz processor [50]. Geometries of the precursor molecules were first optimized at B3LYP and MP2 levels of theory using 6-311++G(d,p) basis set and also at the B3LYP level using aug-cc-pVDZ basis set. Starting from the optimized monomer geometries, the geometry of the 1:1 complexes was then optimized without imposing any constraints. Calculations

were also performed for the higher 1:2 and 2:1 C_2H_2—CH_3CN complexes. Vibrational wavenumber calculations were performed for the optimized geometries to enable us to characterize the nature of the stationary points and also to assign the observed wavenumbers in our matrix isolation experiments. The computed wavenumbers for the different modes were scaled on a mode-by-mode basis for assigning the experimental features. Stabilization energies were computed for the complexes, corrected separately, for basis set superposition errors (BSSE) using the method outlined by Boys and Bernardi [51] and zero point energies.

Bader's atoms-in-molecules (AIM) theory was applied to study the nature of the interaction in the C_2H_2—CH_3CN complexes [52]. We searched for a (3, −1) bond critical point between the C_2H_2 and CH_3CN sub-molecules, which could be associated with the intermolecular interaction using the AIM package [53]. The properties at this BCP, such as the electron density $\rho(r_c)$, $\nabla^2\rho(r_c)$, and the ratio of the eigenvalues $|\lambda_1|/\lambda_3$ were also examined using the AIM package. It is well known that weak van der Waals type interactions are characterized by small values of $\rho(r_c)$ and $\nabla^2\rho(r_c) > 0$ [54]. In order to understand the nature of hyper conjugative charge-transfer interactions in the C_2H_2—CH_3CN complexes, NBO (version 3.1) analysis was performed, invoked through Gaussian [55].

Results and discussions

Experimental details

Fig. 1 (3320–3220 cm^{-1}) and Fig. 2 block A (3270–3200 cm^{-1}) and block B (830–760 cm^{-1}) shows the pre-annealed (soon after deposition) spectra of C_2H_2 with and without CH_3CN in an Ar and N_2 matrices. Fig. 3 block A (3275–3215 cm^{-1}) and block B (800–750 cm^{-1}), Fig. 4 block A (3270–3200 cm^{-1}) and block B (830–760 cm^{-1}) shows the IR spectra obtained after the matrix

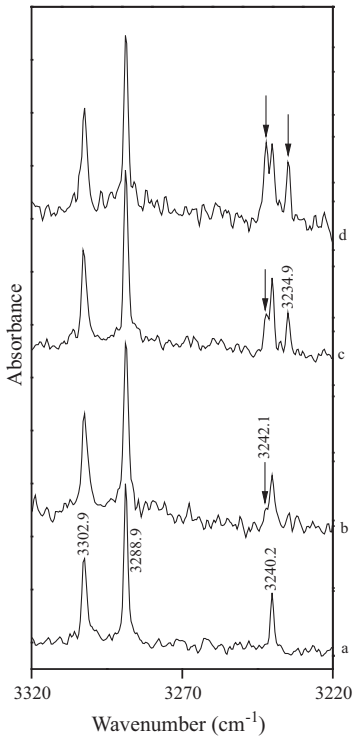

Fig. 1. As deposited spectra of C_2H_2/CH_3CN complex in Ar matrix spanning the region 3320–3220 cm^{-1}. Matrix isolation spectra for various concentrations of $C_2H_2/CH_3CN/Ar$ (a) 0.2/0/1000; (b) 0.1/1.5/1000; (c) 0.2/1.5/1000; (d) 0.1/2.5/1000. Spectra shown here were recorded at 12 K.

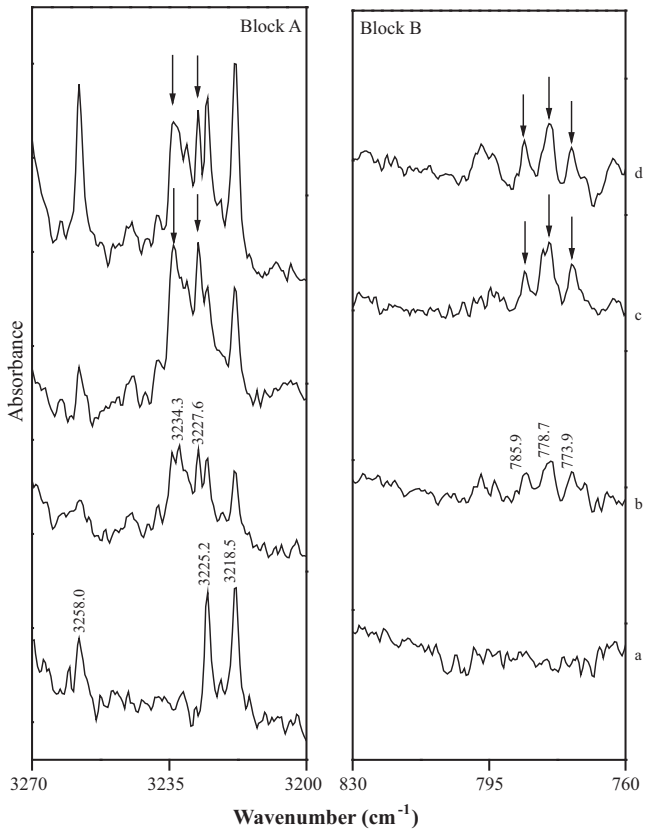

Fig. 2. As deposited spectra of C_2H_2/CH_3CN complex in N_2 matrix spanning the region 3270–3200 (block A) and 830–760 (block B) cm^{-1}. Matrix isolation spectra for various concentrations of $C_2H_2/CH_3CN/N_2$ (a) 0.25/0/1000; (b) 0.25/1.5/1000; (c) 0.25/2.5/1000; (d) 0.5/1.5/1000. Spectra shown here were recorded at 12 K.

were annealed at 35 K (Ar) and 30 K (N_2), respectively. In the Ar matrix, C_2H_2 shows two strong absorptions at 3288.9 and 3302.9 cm^{-1} (Fig. 1a), which have been assigned to components of a Fermi diad involving the ν_3 mode and a combination band ($\nu_2 + \nu_4 + \nu_5$) [56] while the doubly degenerate ν_5 mode of C_2H_2 occurs as a single sharp peak at 736.8 cm^{-1} in an Ar matrix (not shown in figure), whereas the same mode appears as a doublet at 742.0 and 742.7 cm^{-1} in N_2 matrix (not shown in figure) [57]. When C_2H_2 and CH_3CN were co-deposited, new features were observed in the pre-annealed matrix at 3242.1, 3234.9 cm^{-1} in Ar (Fig. 1b–d) and at 3234.3, 3227.6 cm^{-1} in N_2 matrix (Fig. 2b–d, block A). On annealing, the new feature observed in the as-deposited spectrum at 3234.9 cm^{-1} in Ar and 3234.3 and 3227.6 cm^{-1} in N_2 matrix increases in intensity. Further, a new feature starts appearing at 3228.6 cm^{-1} in an Ar matrix, whereas the intensity of the feature observed at 3242.1 cm^{-1} in the as-deposited spectra decreases (Figs. 3b–d and 4b–d, block A). In the ν_5 bending region of C_2H_2 in Ar matrix, only on annealing, new features were observed at 780.6, 783.0 cm^{-1} (Fig. 3c and d, block B) whereas in N_2 matrix, new features observed at 773.9 and 778.7 cm^{-1} (Fig. 4b–d, block B) in the pre-annealed spectra increases in intensity. It may be noted that the feature observed at 3262.8 and 3258.0 cm^{-1} in Ar and N_2 matrices are due to the C_2H_2 dimer. Since, water is an inevitable impurity the feature due to C_2H_2—H_2O complex was observed at 3240.2, 785.5 cm^{-1} in Ar and as a site split doublet at 3218.5, 3225.2, 785.9, 795.1 and 798.0 cm^{-1} in N_2 matrix [57].

Fig. 5 (block A and B) shows the infrared spectra of CH_3CN isolated in Ar and N_2 matrices. The region spanned in this figure is between 2275–2245 cm^{-1}. The features observed at 2258.0 and 2257.5 cm^{-1} are due to ν_2 CN stretching mode of CH_3CN in Ar

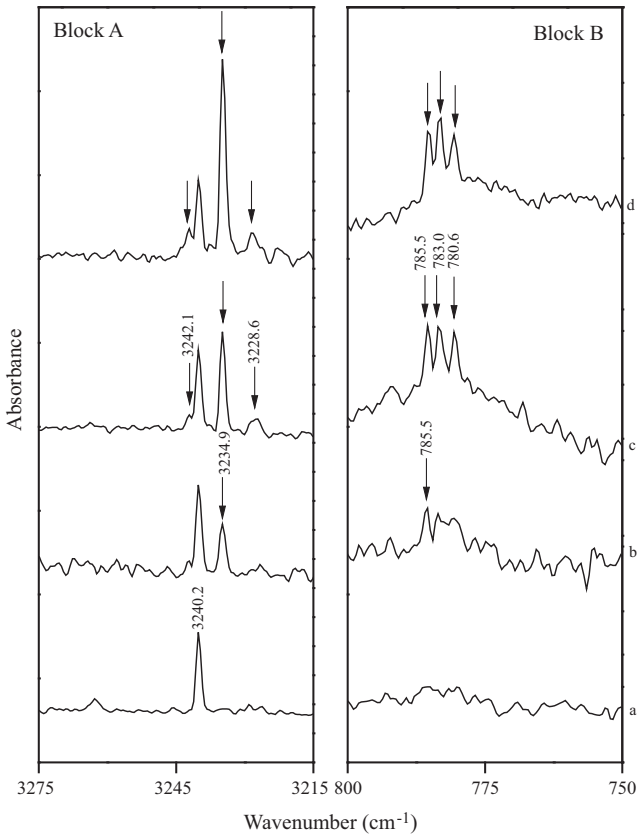

Fig. 3. Spectra of C_2H_2/CH_3CN complex in Ar matrix spanning the region 3275–3215 cm^{-1} (block A) and 800–750 cm^{-1} (block B). Matrix isolation spectra for various concentrations of C_2H_2/CH_3CN/Ar. (a) 0.2/0/1000; (b) 0.1/1.5/1000; (c) 0.2/1.5/1000; (d) 0.1/2.5/1000. Spectra shown here were recorded after annealing the matrix at 35 K.

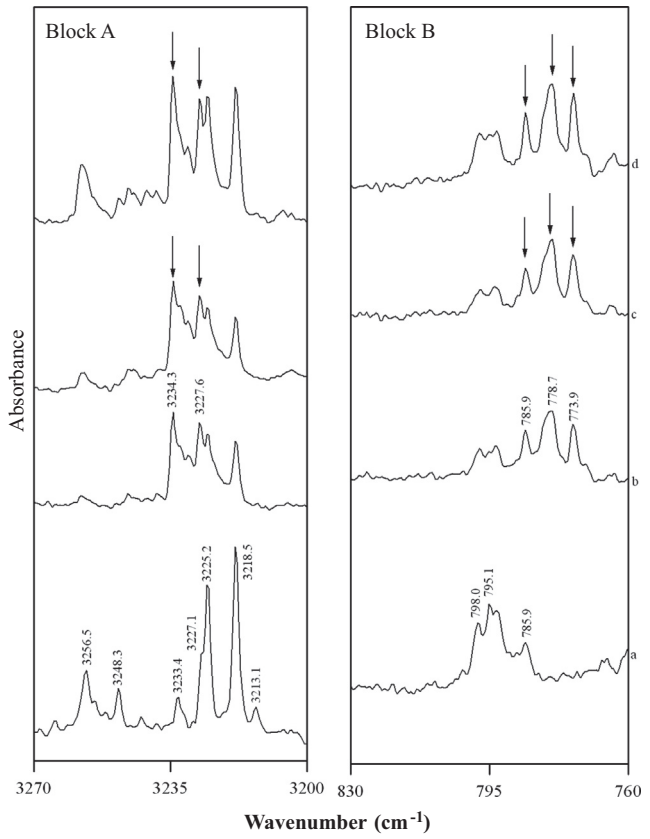

Fig. 4. Spectra of C_2H_2/CH_3CN complex in N_2 matrix spanning the region 3270–3200 (block A) and 830–760 (block B) cm^{-1}. Matrix isolation spectra for various concentrations of $C_2H_2/CH_3CN/N_2$ (a) 0.25/0/1000; (b) 0.25/1.5/1000; (c) 0.25/2.5/1000; (d) 0.5/1.5/1000. Spectra shown here were recorded after annealing the matrix at 30 K.

and N_2 matrices, respectively. The feature observed at 2266.6 cm^{-1} in N_2 matrix is due to CH_3CN monomer in a second site [58]. The features observed at 2256.1 and 2254.1 cm^{-1} are due to $(CH_3CN)_2$ in Ar and N_2 matrices, which agrees well with the literature value [21–23,45,59]. When C_2H_2 and CH_3CN were co-deposited and the matrix then annealed, product absorption band appeared in the ν_5 stretching region as a doublet in an Ar matrix at 2263.8 and 2265.7 cm^{-1} whereas in N_2 matrix new feature was observed at 2261.8 cm^{-1}. It should be mentioned that feature observed at 2272.9 cm^{-1} in N_2 matrix could be due to $CH_3CN—H_2O$ complex.

We could not observe any new features in the ν_4 symmetric CC stretch, ν_7 CH_3 rocking, ν_3 CH_3 deformation, ν_6 antisymmetric CH_3 deformation, ν_1 symmetric CH stretching, ν_5 antisymmetric CH stretching modes of CH_3CN in both Ar and N_2 matrices.

All the features of the product bands appeared only when both the reagents were co-deposited and showed a concentration dependence on the precursors, lending credence to their assignments to the $C_2H_2—CH_3CN$ complexes.

Computations on the 1:1 $C_2H_2—CH_3CN$ complexes

Ab initio computations on the $C_2H_2—CH_3CN$ system at the B3LYP and MP2 level of theory using the 6-311++G(d,p) basis set and B3LYP/aug-cc-pVDZ level of theory yielded only one minima corresponding to C—H···N complex A. Fig. 6 shows the structure for the C—H···N complex A computed at B3LYP/6-311++G(d,p) level of theory. For the complex A, the bond distance between the hydrogen, 7H of C_2H_2 and 6N of CH_3CN is 2.34 Å. The selected bond distances, bond angles and dihedral angles for these complexes are given in Table 1.

The interaction energies for the $C_2H_2—CH_3CN$ complex A with and without ZPE and also with BSSE correction computed at the B3LYP/6-311++G(d,p) and MP2 levels using 6-311++G(d,p) basis set and B3LYP/aug-cc-pVDZ level of theory are given in Table 2. A combined correction for ZPE and BSSE was not calculated as it has been shown to underestimate the bonding enthalpy [59]. From Table 2 it is clear that the formation of complex A is indicated to be exothermic by about 2.6 kcal/mol at MP2/6-311++G(d,p) level with ZPE correction. Although there are deviations in the numerical values of energies with the different basis sets, the trends in the energies are found to be qualitatively similar for the complex A.

Vibrational assignments: $C_2H_2—CH_3CN$ complex A

The experimental vibrational wavenumbers of the $C_2H_2—CH_3CN$ complex A were compared with the wavenumbers calculated using B3LYP/6-311++G(d,p) level of theory (Table 3). The deviations between the experimental and calculated vibrational wavenumbers are attributed to matrix shifts as well as deficiencies of the theoretical model. Scaling factors for each vibrational mode of the C_2H_2 and CH_3CN monomers were calculated to correct these deviations. These scaling factors, by definition, exactly reproduce the experimental values of the monomers (Table 3). Applying scaling factor to the modes of the complexes allows one to reliably predict the band position of the $C_2H_2—CH_3CN$ complex.

ν_3 assymetric stretch of C_2H_2

As mentioned earlier in Ar matrix, two new features were observed at 3242.1 and 3234.9 cm^{-1} in the as-deposited spectrum

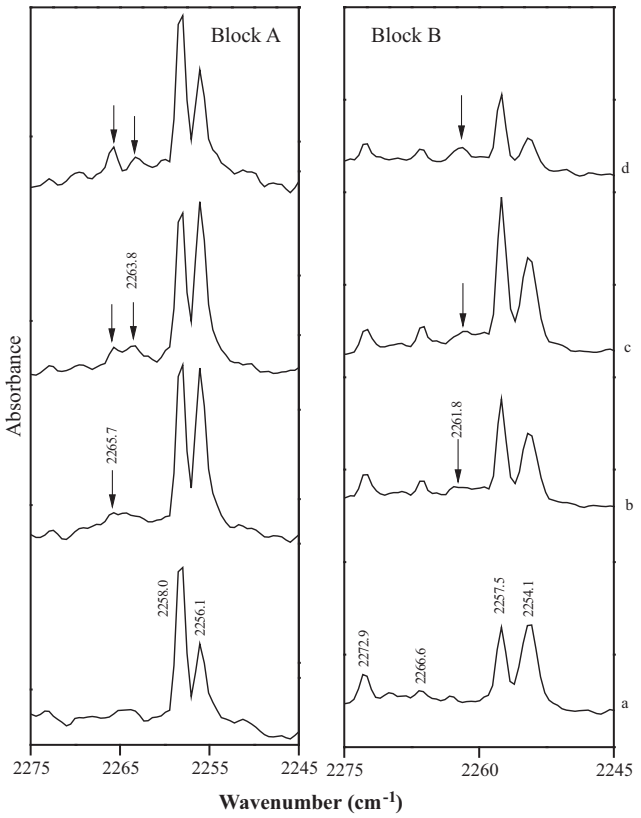

Fig. 5. Spectra of C_2H_2/CH_3CN complex in Ar (block A) and N_2 (block B) matrices spanning the region 2275–2245 cm^{-1}. Matrix isolation spectra for various concentrations of $C_2H_2/CH_3CN/Ar$ (a) 0/2.5/1000; (b) 0.1/2.5/1000; (c) 0.2/2.5/1000; (d) 0.4/2.5/1000 and $C_2H_2/CH_3CN/N_2$ (a) 0/2.5/1000; (b) 0.25/1.5/1000; (c) 0.25/2.5/1000; (d) 0.5/1.5/1000. Spectra shown here were recorded after annealing the matrix at 35 K and 30 K.

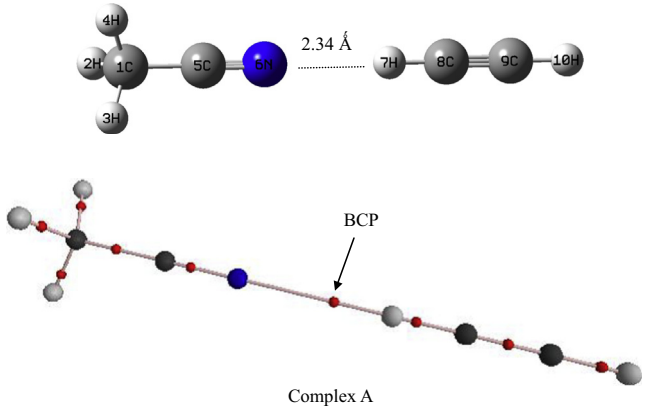

Fig. 6. Computed structure of C_2H_2–CH_3CN complex A at B3LYP/6-311++G(d,p) level of theory.

and the feature observed at 3234.9 cm^{-1} increased in intensity on annealing whereas the intensity of the feature at 3242.1 cm^{-1} slightly decreases. The experimental shifts of these features from the monomer are 46.8 and 54.0 cm^{-1}, respectively, compares well with the scaled computed value of 3243.4 cm^{-1} for the complex A, a shift of 45.5 cm^{-1}. It should be mentioned that the feature observed at 3242.1 cm^{-1} slightly decreased on annealing and could be attributed to site split feature for the complex A in an Ar matrix. In N_2 matrix, a new feature was observed at 3234.3 cm^{-1}, a red shift of 48.3 cm^{-1}, which increases on annealing and agrees well

Table 1
Structural parameters for the C_2H_2—CH_3CN complex A computed at the B3LYP/6-311++G(d,p) level of theory.

Parameter	Complex A
C5—N6	1.1519 (1.1526)
C5—C1	1.4556 (1.4564)
C1—H3	1.0918 (1.0919)
N6—H7	2.3442
C8—H7	1.0687 (1.0626)
C8—C9	1.2008 (1.1993)
H10—C9	1.0627 (1.0626)
∠N6—C5—C1	180.0 (180.0)
∠H7—C8—C9	180.0 (180.0)
∠H4—C1—H3	108.8 (108.8)
∠H4—C1—C5	110.1

Where relevant, the parameters for the monomer are given in brackets.
Bond lengths in Å, and angles in °.

Table 2
Raw[a]/ZPE-corrected/BSSE-corrected interaction energies for the C_2H_2—CH_3CN complexes A–D computed at the B3LYP and MP2 levels of theory using 6-311++G(d,p) basis sets and B3LYP/aug-cc-pVDZ.

Complex	Interaction energy (ΔE)		
	B3LYP/6-311++G(d,p)	MP2/6-311++G(d,p)	B3LYP/aug-cc-pVDZ
A	−2.7/−2.0/−2.5	−3.3/−2.6/−2.7	−3.1/−2.2/−2.5
B	−7.1/−5.6/−3.5	−[b]	−7.7/−6.14/−3.5
C	−4.3/−3.0/−3.4	−7.5/−6.2/−4.4	−5.0/−3.5/−3.5
D	−3.3/−2.2/−2.3	−5.1/−3.8/−2.5	−3.9/−2.6/−2.3

All energies are in kcal/mol (see text for details).
[a] Raw interaction energies refer to energies not corrected for either ZPE or BSSE.
[b] Calculation could not be performed (see text for details).

with the scaled computed shift of 45.2 cm^{-1} for the complex A. The agreement between the experimental and computed wavenumbers supports the computationally derived C—H···N structure of the complex, with C_2H_2 being the proton donor.

The assignments for the feature observed at 3228.6 and 3227.6 cm^{-1} in Ar and N_2 matrices will be discussed in the later section.

ν_5 mode of C_2H_2

The ν_5 mode of the C_2H_2 sub-molecule in the complex A in an Ar and N_2 matrix was computed to occur at 796.0 and 804.6 cm^{-1}, a blue shift of 59.2 and 59.9 $cm^{-1}$from the computed feature for the same mode in free C_2H_2. A feature was experimentally observed in an Ar and N_2 matrix at 780.6 and 773.9 cm^{-1}, which is in close agreement with our computations.

ν_2 CN stretching mode of CH_3CN

This mode of CH_3CN sub-molecule was observed as a *site-split* doublet feature at 2263.8/2265.7 and 2261.8 cm^{-1}, a blue shift of 5.8/7.7, 4.3 cm^{-1} in an Ar and N_2 matrices, which compares well with the scaled computed value for the complex A, a blue shift of 5.6 and 6.5 cm^{-1} in Ar and N_2 matrices, respectively.

Computations on the higher $C_2H_2CH_3CN$ complexes

To find out the possible sites of attack of the next C_2H_2 or CH_3CN molecule on the C_2H_2—CH_3CN complex *ab initio* computations were carried out for the higher complexes. One minimum energy structure with C_2H_2—$(CH_3CN)_2$ (complex B) was obtained in the potential energy surface while two minima were found for $(C_2H_2)_2$—CH_3CN (complexes C and D). Fig. 7 shows the structure

Table 3
Computed unscaled and scaled vibrational wavenumbers, scaling factors, and mode assignments computed at the B3LYP/6-311++G(d,p) level and comparison with experimental wavenumbers for the C_2H_2—CH_3CN complexes A–D in an Ar and N_2 matrices.

Computed/unscaled ν (cm^{-1})	Ar			N_2			Mode assignment
	Computed/scaled ν (cm^{-1})	Scaling factor	Exp ν (cm^{-1})	Computed/scaled ν (cm^{-1})	Scaling factor	Exp ν (cm^{-1})	
Acetonitrile							
930.0 (2)[a]	917.2	0.9856	916.6	917.6	0.9967	917.6	ν_4 sym. CC str. (A_1)
1061.0 (2)	1038.2	0.9785	1038.2	1043.3	0.9833	1040.7/1045.8	ν_7 CH_3 rock (E)
1411.6 (3)	1375.9	0.9747	1375.9	1378.5	0.9766	1378.5	ν_3 sym. CH_3 def (A_1)
1474.7 (12)	1445.5	0.9802	1445.5	1447.9	0.9818	1446.7/1449.1	ν_6 antisym. CH_3 def. (E)
2362.9 (12)	2258.0	0.9556	2258.0	2257.5	0.9554	2257.5	ν_2 CN str. (A_1)
3045.9 (4)	2950.6	0.9687	2950.5	2949.0	0.9682	2949.0	ν_1 sym. CH str. (A_1)
3115.6 (1)	3004.4	0.9643	3004.5	3009.3	0.9659	3009.3	ν_5 antisym. CH str. (E)
Acetylene							
3420.6 (94)	3288.9	0.9615	3288.9	3282.6	0.9597	3282.6	ν_3 C—H antisym. str. mode
772.7 (112)	736.8	0.9535	736.8	744.7	0.9638	742.0/747.4	ν_5 C—H bending mode
Complex A							
3373.3 (314)	3243.4	0.9615	3234.9/3242.1	3237.4	0.9597	3234.3	ν_3 antisym. C—H str. mode
834.8 (90)	796.0	0.9535	780.6	804.6	0.9638	773.9	ν_5 C—H bending mode
834.8 (90)	796.0			804.6			
2368.8 (20)	2263.6	0.9556	2265.7/2263.8	2264.1	0.9554	2261.8	ν_2 CN str. mode
Complex B							
3366.6 (319)	3237.0	0.9615	3228.6	3237.0	0.9597	3227.6	ν_3 antisym. C—H str. mode
835.2 (82)/838.1 (101)	796.4/799.1	0.9535	780.6/783.0	805.0/807.8	0.9638	773.9/778.7	ν_5 C—H bending mode
2361.2 (36)/2357.0 (15)	2256.4/2252.4	0.9556	–[b]	2255.9/2251.9	0.9554	–[b]	ν_2 CN str. mode
Complex C							
3371.8 (227)/3389.9 (194)	3242.0/3259.4	0.9615	–[b]	3235.9/3253.3	0.9597	–[b]	ν_3 antisym. C—H str. mode
796.6 (47)	759.5	0.9535	–[b]	767.8	0.9638	–[b]	ν_5 C—H bending mode
807.6 (95)	770.1			778.4			
822.9 (118)	784.6			793.1			
827.0 (127)	788.5			797.0			
2363.8 (20)	2258.9	0.9556	–[b]	2258.4	0.9554	–[b]	ν_2 CN str. mode
Complex D							
3368.5 (391)/3418.1 (98)	3238.8	0.9615	–[b]	3232.7	0.9597	–[b]	ν_3 antisym. C—H str. mode
	3286.5						
773.6 (93)	737.6	0.9535	–[b]	745.6	0.9638	–[b]	ν_5 C—H bending mode
779.0 (126)	742.8			750.8			
838.1 (100)	799.1			807.8			
841.0 (83)	801.9			810.6			
2363.8 (21)	2258.8	0.9556	–[b]	2258.4	0.9554	–[b]	ν_2 CN str. mode

Computations were performed at the B3LYP/6-311++G(d,p) level.
[a] Computed infrared intensities (km/mol) are given in parentheses.
[b] Experimental features were not observed.

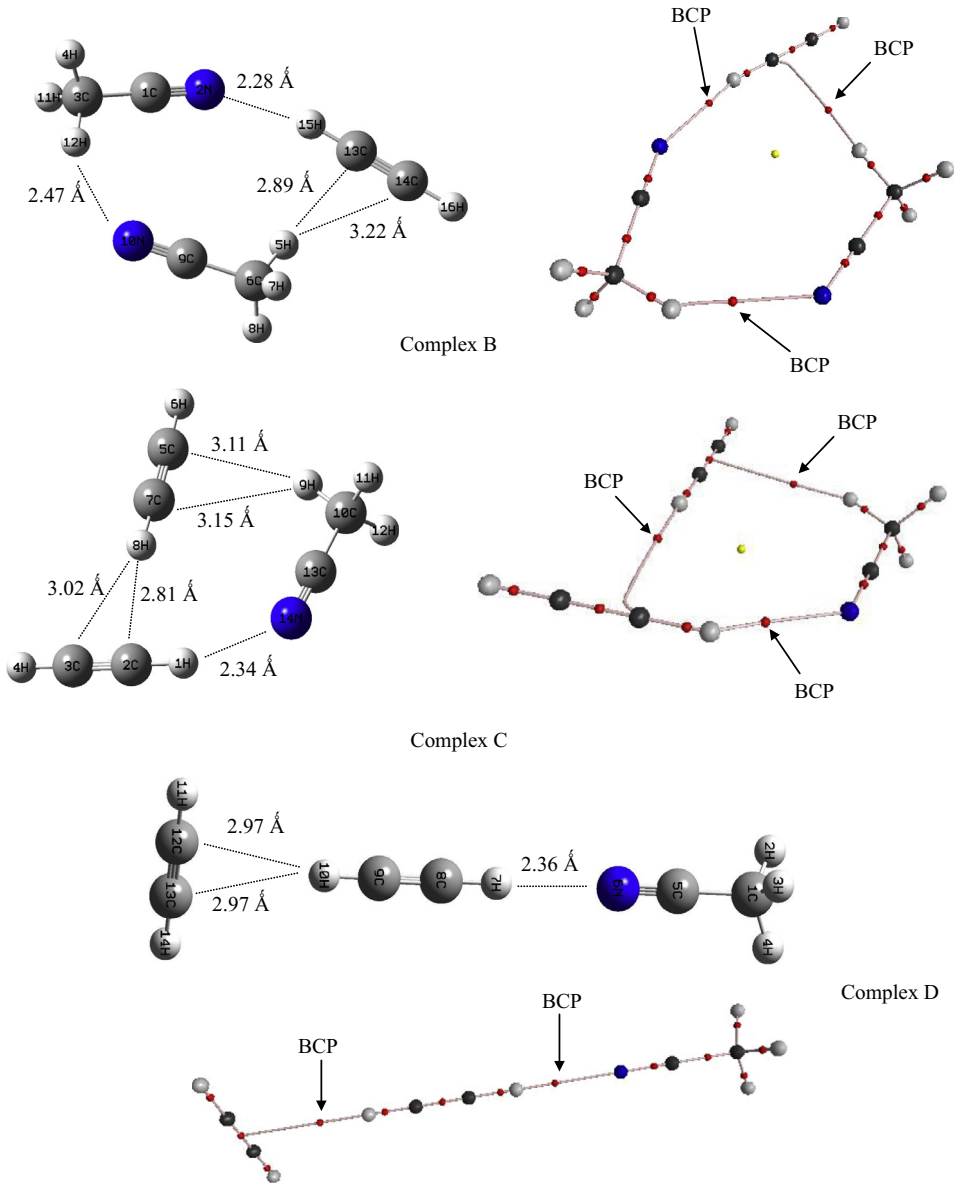

Fig. 7. Computed structure of C_2H_2–CH_3CN complexes B–D at B3LYP/6-311++G(d,p) level of theory.

of these complexes calculated at B3LYP/6-311++G(d,p) level of theory. The higher complexes B–D shown in Fig. 7 are stabilized by both C—H···N and C—H···π interactions.

Table 2 gives the stabilization energies for the higher complexes B–D at B3LYP and MP2 levels of theory using 6-311++G(d,p) basis sets and B3LYP/aug-cc-pVDZ level of theory. The ZPE-corrected energy for complex B is exothermic by 5.6 kcal/mol at B3LYP/6-311++G(d,p) level. We could not perform computations at MP2/6-311++G(d,p) level of theory for the complex B due to limited computational resources. It is well known that CH_3CN forms dimer in the gas phase and the structure of the dimer is well documented [22]. $(CH_3CN)_2$ forms a cyclic dimer with C—H···N interaction between the two CH_3CN molecules [25]. When C_2H_2 interacts with the $(CH_3CN)_2$ (complex B) the hydrogen 5H of CH_3CN interacts with the carbons 13C and 14C of C_2H_2, the bond distances are 2.89 Å and 3.22 Å respectively and the nitrogen 2N of CH_3CN interacts with the hydrogen 15H of C_2H_2, a bond distance of 2.28 Å (Table 4). Further, there is yet another interaction between the hydrogen 12H and nitrogen 10N between the two acetonitrile, a bond distance of 2.47 Å making a ten membered cyclic structure. In complex B, there are two C—H···N interactions and one C—H···π interaction. Due to these interactions, the C—H bond of C_2H_2 submolecule is elongated by 0.0078 Å, which results in a red shift of 54.0 cm^{-1} at B3LYP/6-311++G(d,p) level.

In complex C, the hydrogen 1H of C_2H_2 interacts with 14N of CH_3CN, the hydrogen 9H of CH_3CN interacts with π cloud of C_2H_2 (5C and 7C carbons) and the hydrogen 8H of C_2H_2 interacts with the π cloud of C_2H_2 (2C and 3C carbons) giving a nine membered cyclic structure. In complex C, there are two C—H···π interaction and one C—H···N interaction, due to this interaction the C—H bond is lengthened by 0.0056 Å and red shifted by 46.9 and 29.5 cm^{-1}, respectively.

Complex D has a linear structure with one C—H···N and C—H···π interaction. The bond distance between the 6N and 7H is 2.36 Å further, there is a interaction between the hydrogen 10H of C_2H_2 with the carbons 12C and 13C of C_2H_2 and the bond distances are 2.97 Å. The C—H bond is red shifted by 50.1 and 2.4 cm^{-1} and the C—H bonds are lengthened by 0.0053 Å and 0.0014 Å respectively. Among the complexes C and D, C is more stable than D since the ZPE corrected energy of complex C is

Table 4
Structural parameters for the C_2H_2—CH_3CN complexes B–D computed at B3LYP/6-311++G(d,p) level of theory.

Parameter	Complex B	Parameter	Complex C	Parameter	Complex D
C1—N2	1.1526	H1—C2	1.0687	C5—N6	1.1520
N2—H15	2.2791	H1—N14	2.3396	N6—H7	2.3602
N10—H12	2.4715	H8—C2	2.8149	H10—C12	2.9738
H5—C13	2.8911	H8—C3	3.0172	H10—C13	2.9744
H5—C14	3.2156	H9—C7	3.1467	C1—C5	1.4557
∠C1—N2—H15	154.1	H9—C5	3.1130	C1—H2	1.0918
∠C9—N10—H12	133.9	∠N14—H1—C2	155.3	∠C5—N6—H7	179.9
∠H5—C13—H15	87.5	∠C13—N14—H1	135.0	∠C9—H10—C13	168.4
∠N10—H12—C3	144.1	∠C10—H9—C7	136.6	∠C9—H10—C12	168.3
tor∠C1—N2—H15—C13	0.27	∠C10—H9—C5	158.7	∠H2—C1—H4	110.1
tor∠C9—N10—H12—C3	−0.08	∠C7—H8—C2	169.9	∠H3—C1—H2	108.8
tor∠C6—H5—C13—H15	0.15	tor∠C2—H1—N14—C13	−0.08	tor∠H3—C1—C5—N6	4.76
tor∠C6—H5—C14—C13	179.6	tor∠C10—H9—C7—H8	−0.18	tor∠C5—N6—H7—C8	1.97
tor∠C14—C13—H15—N2	2.0	tor∠C7—H8—C2—H1	−0.05	tor∠C9—H10—C12—C13	179.7

Bond lengths in Å, angles and torsional angles in °.

exothermic by about 3.0 kcal/mol at B3LYP/6-311++G(d,p) level of theory relative to complex D. This could be due to the fact that complex C is stabilized by two intermolecular C—H···π interaction and one C—H···N interaction whereas complex D with an open and linear structure, stabilized only by intermolecular C—H···π and C—H···N interactions.

Vibrational assignments: C_2H_2—CH_3CN higher complexes

At higher concentrations of CH_3CN in Ar and N_2 matrices, new features were observed in the spectra and the intensity of the absorption band increases with the CH_3CN concentration, indicating that more than one molecule of CH_3CN is involved in the complex. In both the matrices, new absorption peaks were observed at 3228.6 and 3227.6 cm^{-1}, which are assigned to the ν_3 mode of C_2H_2 sub-molecule in the C_2H_2—$(CH_3CN)_2$ complex B. The experimentally observed red shift of the C—H antisymmetric stretching vibration of 60.3 and 55.0 cm^{-1} in Ar and N_2 matrices, which is in good agreement with the calculated shift of 51.9 cm^{-1} for the complex B computed at B3LYP/6-311++G(d,p) level of theory. The ν_5 bending mode of C_2H_2 submolecule for the complex B was computed to occur at 796.1, 799.4 and 805.0, 807.8 cm^{-1}, in an Ar and N_2 matrices, respectively. These features compare well with the experimental feature were observed at 780.6, 783.0 cm^{-1} in Ar and 773.9 785.9 cm^{-1} in N_2 matrix, respectively. It should be mentioned that the feature observed at 780.6 cm^{-1} in Ar and 773.9 cm^{-1} in N_2 matrix in the ν_5 bending mode of C_2H_2 submolecule is assigned for the complex A could also be assigned for the complex B because the computed wavenumbers are very close for the complexes A and B and there is some probability that the bending mode of these complexes can get overlapped.

Nature of the interaction

AIM calculation

To analyze the nature of the interaction in C_2H_2—CH_3CN complexes, AIM theory was used [52]. A (3, −1) bond critical point (BCP) was sought, using the optimized geometry of the C_2H_2—CH_3CN complexes A–D computed at B3LYP/6-311++G(d,p) level of theory. The locations of the bond critical points are shown in Figs. 6 and 7. Table 5 gives the properties of BCP for all the complexes computed at B3LYP/6-311++G(d,p) level of theory. At the BCP for all the complexes A–D, electron density ($\rho(r_c)$), Laplacian of electron density ($\nabla^2\rho(r_c)$) were examined. At the BCP for all the complexes the values of $\rho(r_c)$ are of the order of 10^{-2} au and $\nabla^2\rho(r_c)$ values are positive, as are typical of closed shell interactions [54].

NBO analysis

NBO analysis was carried out to correlate the red-shifted H-bonding with the extent of charge-transfer hyperconjugative interactions. The NBO analysis is a useful tool and provides insight on the nature of the interactions particularly of red-shifted type [60–73]. The stabilizing interactions that arise due to the hyperconjugative interaction (n–σ*) in the H-bonded complexes is responsible for the origin of bond lengthening, which results in a red shift of vibrational wavenumber.

In NBO analysis, off-diagonal elements of the Fock matrix in the NBO basis give the measure of delocalization effects. The second-order perturbation energy (E_2) gives an estimate of the strength of these delocalization interactions.

Table 6 shows the results of NBO analysis of C_2H_2—CH_3CN complexes A–D computed at B3LYP/6-311++G(d,p) level of theory. From the table it is clear that for the complex A, the dominant part of the electron density transfer (EDT) occurs from the n^1N6 lone pair to anti bonding σ* orbital of the H7—C8 of C_2H_2 sub-molecule, which is evident from the increase in the electron occupancy of antibonding σ*(H7—C8) orbital of C_2H_2 sub-molecule (by about ∼0.007e) and decrease in the occupancy of donor lone pair on N6 (by about ∼0.006e) in complex A relative to the corresponding monomers. The delocalization of the electron density to the anti bonding, σ*(H7—C8) orbital of C_2H_2 weakens the C—H bond, resulting in elongation of the C—H bond and a concomitant red shift of its C—H stretching frequency. The second order perturbation E_2 energy for the delocalization interaction was found out to be ∼3.30 kcal/mol.

In Complex B, there are two C—H···N and one C—H···π interactions. The hyperconjugative interaction between the n^1N6 → σ*(H9—C7) and n^1N12 → σ*(H13—C14) are the dominant interactions. The second order perturbation E_2 energy for the above delocalization interactions were found to be ∼1.17 and ∼3.77 kcal/mol, respectively. Due to the hyperconjugative interaction the electron occupancy in the antibonding orbital of σ*(H9—C7) and σ*(H13—C14) increases making the C—H bond to lengthen and concomitant red shift in the C—H frequency. The next dominant interaction in the complex B was found to be the π_1(C14—C15) → σ*(H4—C1) as the E_2 energy for this interaction was calculated to be 0.64 kcal/mol. In addition to the above interactions, we also observed in the complex B that the stabilization arises due to the *bond pair–acceptor orbital interaction* such as σ(C7—H9) → π*(C5—N6), π_2(C5—N6) → σ*(C7—H9), σ(C14—H13) → π_1^*(C11—N12) and π_1(C11—N12) → σ*(C14—H13) whose magnitudes are smaller than lone pair-acceptor orbital interactions but still cannot be neglected.

Table 5
Properties of intermolecular (3, −1) bond critical point in C_2H_2—CH_3CN complexes A–D computed at B3LYP/6-311++G(d,p) level of theory.

Complexes		$\rho(r_C)$	$\nabla^2\rho\ (r_C)$	λ_1	λ_2	λ_3	$\lvert\lambda_1\rvert/\lambda_3$
Complex A	C≡N (AN)...H (C_2H_2)	0.01107	0.08339	−0.01111	−0.01111	0.06117	0.18162
Complex B	C≡N (AN)...H (C_2H_2)	0.01284	0.04552	−0.01337	−0.01330	0.07221	0.18419
	C—H (AN)...N≡C (CH_3CN)	0.00968	0.03068	−0.00894	−0.00864	0.04824	0.18532
	C—H (AN)...π (C_2H_2)	0.00492	0.01220	−0.00343	−0.00286	0.01852	0.18520
Complex C	C≡N (AN)...H (C_2H_2)	0.01121	0.03882	−0.01110	−0.01086	0.06078	0.18263
	C—H (AN)...π (C_2H_2)	0.00403	0.00991	−0.00264	−0.00209	0.01464	0.18033
	C—H (Ac)...π (C_2H_2)	0.00528	0.01352	−0.00377	−0.00306	0.02035	0.18526
Complex D	C≡N (AN)...H (C_2H_2)	0.01071	0.03746	−0.01064	−0.01064	0.05874	0.18114
	C—H (Ac)...π (C_2H_2)	0.00460	0.01169	−0.00314	−0.00251	0.01734	0.18108

Table 6
Electron occupancies of various NBOs of C_2H_2—CH_3CN complexes A–D computed at B3LYP/6-311++G(d,p) level of theory. The donor–acceptor delocalization interaction and delocalization energies (E_2, kcal/mol) are also shown.

Complexes	NBO	Occupancy	Donor–acceptor delocalization interaction	Second order perturbation (E_2) energy (kcal/mol)
Complex-A	n^1N6	1.96405 (1.96988)[a]	n^1N6 → σ*(H7—C8)	3.30
	σ*(H7—C8)	0.01311 (0.00600)[b]		
Complex-B	n^1N6	1.96738 (1.96988)[a]	n^1N6 → σ*(H9—C7)	1.17
	σ*(H9—C7)	0.01068 (0.00832)[a]	σ(C7—H9) → π*(C5—N6)	0.21
			π_2(C5—N6) → σ*(C7—H9)	0.24
	σ(C7—H9)	1.96593 (1.97097)[a]		
	π_2^*(C5—N6)	0.03998 (0.03563)[a]		
	n^1N12	1.96188 (1.96988)[a]	n^1N12 → σ*(H13—C14)	3.77
	σ*(H13—C14)	0.01511 (0.00600)[b]		
	π_1(C11—N12)	1.98828 (1.98709)[a]	π_1(C11—N12) → σ*(C14—H13)	0.19
			σ(C14—H13) → π_1^*(C11—N12)	0.12
	σ(C14—H13)	1.98901 (1.99054)[b]		
	π_1^*(C11—N12)	0.04043 (0.03563)[a]		
	π_1(C14—C15)	1.99177 (1.99961)[b]	π_1(C14—C15) → σ*(H4—C1)	0.64
	σ*(H4—C1)	0.00933 (0.00832)[a]		
Complex-C	n^1N14	1.96430 (1.96988)[a]	n^1N14 → σ*(H1—C2)	2.28
	σ*(H1—C2)	0.01262 (0.00600)[b]		
	π_2(C13—N14)	1.98676 (1.98709)[a]	π_2(C13—N14) → σ*(C1—H2)	0.42
	σ(H1—C2)	1.98885 (1.99054)[b]		
	π_2^* (C13—N14)	0.03887 (0.03563)[a]	σ(C1—H2) → π_2^*(C13—N14)	0.23
	π_2(C2—C3)	1.99137 (1.99961)[b]	π(C2—C3) → σ*(H8—C7)	0.98
	σ*(H8—C7)	0.00871 (0.00600)[b]		
	π_1(C5—C7)	1.99712 (1.99961)[b]	π_1(C5—C7) → σ*(H9—C10)	0.33
	σ*(H9—C10)	0.00888 (0.00832)[b]		
Complex-D	n^1N6	1.96441 (1.96988)[a]	n^1N6 → σ*(H7—C8)	3.11
	σ*(H7—C8)	0.01272 (0.00600)[b]		
	π_2(C12—C13)	1.99135 (1.99961)[b]	π_2(C12—C13) → σ*(C9—H10)	0.77
	σ*(C9—H10)	0.00823 (0.00600)[b]		

[a] Occupancy of monomeric CH_3CN is given in parenthesis.
[b] Occupancy of monomeric C_2H_2 is given in parenthesis.

In complex C, there is one C—H···N and two C—H···π interactions. The n^1N14 → σ*(H1—C2) hyperconjugative interaction is the strongest and the perturbation energy E_2 is ∼2.28 kcal/mol. The magnitude of second order perturbation energy E_2 for the *bond pair–acceptor orbital interaction* such as π(C2—C3) → σ*(H8—C7), π_2(C13—N14) → σ*(C1—H2), π_1(C5—C7) → σ*(H9—C10) and σ(C1—H2) → π_2^*(C13—N14) are 0.98,0.42,0.33 and 0.23 kcal/mol respectively.

In complex D the dominant interaction is n^1N6 → σ*(H7—C8) the second order perturbation energy E_2 is ∼3.11 kcal/mol. There is a weak π_2(C12—N13) → σ*(C9—H10) interaction. Even though, the complexes C and D are isomeric to each other, the cyclic nature of the complex C ensures larger number of hyperconjugative delocalization interactions relative to complex D, which are responsible in making the complex C energetically more favorable than complex D. It is clear from the above arguments that hyperconjugative interactions play a major role in the stabilization of the C_2H_2—CH_3CN complexes.

The consideration of the charge transfer hyperconjugative interaction alone is insufficient in describing the stabilization of the hydrogen-bonding interaction, the other effects such as electrostatic, polarization, and dispersion also play an important role. Nevertheless, hyperconjugative delocalization interactions predict the stability of different hydrogen-bonded complexes with reasonable accuracy.

Conclusions

The highlight of the present work is the identification of the 1:1 C—H···N complex formed between C_2H_2 and CH_3CN, which was recorded for the first time in an Ar and N_2 matrices. The formation of this complex was evidenced from the red and blue shifts in the wavenumbers corresponding to the C—H stretching and bending modes of C_2H_2 and blue shifts in the CN stretching modes of CH_3CN sub-molecules. We have also found evidences for the formation of 1:2 C_2H_2—CH_3CN higher complexes in an Ar and N_2 matrices. The

experimental observations agreed well with the computations performed for these complexes at the B3LYP levels of theory using 6-311++G(d,p) basis set. AIM and NBO analyses clearly predicted the nature of interaction between the hydrogen bonded sub-molecules in the various C_2H_2—CH_3CN complexes.

Acknowledgement

R. Gopi gratefully acknowledges the Grant of a research fellowship from the IGCAR, Department of Atomic Energy, India.

References

[1] J.E. Del Bene, Hydrogen bonding, in: P. von R. Schleyer (Ed.), The Encyclopaedia of Computational Chemistry, Wiley, New York, 1998, p. 1263.
[2] G.A. Jeffrey, W. Saenger, Hydrogen Bonding in Biological Structures, Springer, Berlin, 1991.
[3] G.C. Pimentel, A.L. McClellan, Annu. Rev. Phys. Chem. 22 (1971) 22347.
[4] P.L. Huyskens, W.A.P. Luck, T. Zeegers-Huuyskens, Intermolecular Forces, Springer-Verlag, Berlin, 1991.
[5] A. Jabalmeli, N.U. Zhanpeisov, A. Znowek, R.H. Sullivan, J. Leszczynski, J. Phys. Chem. 101 (1997) 3619.
[6] A. Engdahl, B. Nelander, Chem. Phys. Lett. 100 (1983) 129.
[7] M.L.H. Jeng, B.S. Ault, J. Phys. Chem. 94 (1990) 1323.
[8] S.A. McDonald, G.L. Johnson, B.W. Keelan, L. Andrews, J. Am. Chem. Soc. 102 (1980) 2892.
[9] A. Engdahl, B. Nelander, Chem. Phys. Lett. 113 (1985) 49.
[10] L. Andrews, G.L. Johnson, B.J. Kelsall, J. Am. Chem. Soc. 104 (1982) 6180.
[11] L. Andrews, G.L. Johnson, B.J. Kelsall, J. Chem. Phys. 76 (1982) 5767.
[12] M.K. Van Bael, J. Smets, K. Schoone, L. Houben, W. McCarthy, L. Adamowicz, M.J. Nowak, G. Maes, J. Phys. Chem. 101 (1997) 2397.
[13] S.W. Han, K. Kim, J. Phys. Chem. 100 (1996) 17124.
[14] X.K. Zhang, E.G. Lewars, R.E. March, J.M. Parnis, J. Phys. Chem. 97 (1993) 4320.
[15] G.A. Jeffrey, An Introduction to Hydrogen Bonding, Oxford University Press, Oxford, 1997.
[16] E.D. Jemmis, K.T. Giju, K. Sundararajan, K. Sankaran, V. Vidya, K.S. Viswanathan, J. Leszczynski, J. Mol. Struct. 510 (1999) 59.
[17] K. Sundararajan, K. Sankaran, K.S. Viswanathan, A.D. Kulkarni, S.R. Gadre, J. Phys. Chem. A 106 (2002) 1504.
[18] K. Sundararajan, K.S. Viswanathan, A.D. Kulkarni, S.R. Gadre, J. Mol. Struct. 613 (2002) 209.
[19] K. Sundararajan, K. Sankaran, K.S. Viswanathan, J. Mol. Struct. 733 (2004) 187.
[20] Orland W. Kolling, Anal. Chem. 59 (1987) 674.
[21] T.B. Freedman, E.R. Nixon, Spectrochim. Acta 28A (1972) 1375.
[22] Hack Sung Kim, Kwan Kim, Bull. Korean Chem. Soc. 13 (1992) 521.
[23] A. Givan, A. Loewenschuss, J. Mol. Struct. 98 (1983) 231.
[24] S. Coussan, Y. Boutelier, J.P. Perchard, V. Brenner, P. Millié, W.Q. Zheng, F. Talbot, J. Chem. Phys. 110 (1999) 10046.
[25] E. Kryachko, M.T. Nguyen, J. Phys. Chem. A 106 (2002) 4267.
[26] S.C. White, H.W. Thompson, Proc. R. Soc. London A 291 (1966) 460.
[27] M.S. Sousa Lopes, H.W. Thompson, Spectrochim. Acta 24A (1968) 1367.
[28] S.S. Mitra, J. Chem. Phys. 36 (1962) 3286.
[29] A. Allerhand, P. von R. Schelyer, J. Am. Chem. Soc. 85 (1963) 371.
[30] N.P. Wells, J.A. Phillips, J. Phys. Chem. A 106 (2002) 1518.
[31] R. Hattori, E. Suzuki, K. Shimizu, J. Mol. Struct. 750 (2005) 123.
[32] Doo-Sik Ahn, Sungyul Lee, Bull. Korean Chem. Soc. 24 (2003) 545.
[33] A. Chaudhari, S. Lee, Int. J. Quantum Chem. 102 (2005) 106.
[34] A.K. Lyashchenkoa, V.S. Dunyashev, Russ. J. Phys. Chem. A 88 (2014) 271.
[35] J.E. Bertie, Z. Lan, J. Phys. Chem. B 101 (1997) 4111.
[36] T. Takamuku, M. Tabata, A. Yamaguchi, J. Nishimoto, M. Kumamoto, H. Wakita, T. Yamaguchi, J. Phys. Chem. B 102 (1998) 8880.
[37] G.M. Chaban, J. Phys. Chem. A 108 (2004) 4551.
[38] R.D. Mountain, J. Phys. Chem. A 103 (1999) 10744.
[39] K.S. Rutkowski, S.M. Melikova, J. Janski, A. Koll, Chem. Phys. 375 (2010) 92.
[40] Małgorzata Domagała, Sławomir J. Grabowski, Chem. Phys. 363 (2009) 42.
[41] Nicola Goldberg, Sarah R. Lubell, Bruce S. Ault, J. Mol. Struct. 740 (2005) 125.
[42] Ryuichi Hattori, Eiichi Suzuki, Kenji Shimizu, J. Mol. Struct. 750 (2005) 123.
[43] Alexander B. Baker, Cindy Samet, Jonathan T. Lyon, Lester Andrews, J. Phys. Chem. A 109 (2005) 8280.
[44] M.P. Bernstein, S.A. Sandford, L.J. Allamandola, APJ 476 (1997) 932.
[45] Louise Schriver, Andre Schriver, Serge Racine, Jean-Pierre Perchard, Chem. Phys. 119 (1988) 95.
[46] Y. Gu, T. Kar, S. Scheiner, J. Mol. Struct. 552 (2000) 17.
[47] William P. Schroeder, Kimberly Chenoweth, Clifford E. Dykstra, Chem. Phys. Lett. 373 (2003) 8.
[48] Elsa Sanchez-Garcıa, Artur Mardyukov, Adem Tekin, Rachel Crespo-Otero, Luis A. Montero, Wolfram Sander, Georg Jansen, Chem. Phys. 343 (2008) 168.
[49] E.L. Zins, L. Krim, Phys. Chem. Chem. Phys. 16 (2014) 3388.
[50] M.J. Frisch, G.W. Trucks, H.B. Schlegel, P.M.W. Gill, B.G. Johnson, M.A. Robb, J.R. Cheeseman, T. Keith, G.A. Petersson, J.A. Montgomery, K. Raghavachari, M.A. Al-Laham, V.G. Zakrzewski, J.V. Ortiz, J.B. Foresman, J. Cioslowski, B.B. Stefanov, A. Nanayakkara, M. Challacombe, C.Y. Peng, P.Y. Ayala, W. Chen, M.W. Wong, J.L. Andres, E.S. Replogle, R. Gomperts, R.L. Martin, D.J. Fox, J.S. Binkley, D.J. Defrees, J. Baker, J.P. Stewart, M. Head-Gordon, C. Gonzalez, J.A. Pople, GAUSSIAN 94, Revision D.1, Gaussian Inc., Pittsburgh, PA, 1995.
[51] S.F. Boys, F. Bernardi, Mol. Phys. 19 (1970) 553.
[52] R.F.W. Bader, Atoms in Molecules. A Quantum Theory, Clarendon Press, Oxford, 1994.
[53] F. Biegle-Koning, R.F.W. Bader, W.-H. Tang, J. Comput. Chem. 96 (2000) 6796. AIM 2000, Version 1.
[54] R.G.A. Bone, R.F.W. Bader, J. Phys. Chem. 100 (1996) 10892.
[55] E.D. Glendening, J.E. Carpenter, F. Weinhold, NBO version 3.1.
[56] R.J. Bemish, P.A. Block, L.G. Pederson, W. Yang, R.E. Miller, J. Chem. Phys. 99 (1993) 8585.
[57] K. Sundararajan, K.S. Viswanathan, J. Mol. Struct. 798 (2006) 109.
[58] Louise Schriver, Andre Schriver, Jean-Pierre Perchard, J. Chem. Soc., Faraday Trans. 81 (1985) 1407.
[59] L. Turi, J. Dannenberg, J. Phys. Chem. 97 (1993) 7899.
[60] F. Weinhold, J. Mol. Struct. (Theochem.) 398 (1997) 181.
[61] G.L. Sosa, N.M. Peruchena, R.H. Conteras, E.A. Castro, J. Mol. Struct. (Theochem.) 577 (2002) 219.
[62] P. Kolandaivel, V. Nirmala, J. Mol. Struct. 694 (2004) 33.
[63] Y.X. Lu, J.W. Zou, Y.H. Wang, Y.J. Jiang, Q.S. Yu, J. Phys. Chem. A 111 (2007) 10781.
[64] W. Wang, P. Hobza, J. Phys. Chem. A 112 (2008) 4114.
[65] N.J.M. Amezaga, S.C. Pamies, N.M. Peruchena, G.L. Sosa, J. Phys. Chem. A 114 (2010) 552.
[66] W. Wang, J. Phys. Chem. A 115 (2011) 9294.
[67] M. Jablonski, M. Palusiak, J. Phys. Chem. A 116 (2012) 2322.
[68] M. Solimannejad, M. Malekani, J. Phys. Chem. A 117 (2013) 5551.
[69] W. Zierkiewicz, D. Michalska, Z. Havlas, P. Hobza, ChemPhysChem 3 (2002) 511.
[70] P. Hobza, Z. Havlas, Theor. Chem. Acc. 108 (2002) 325.
[71] W. Zierkiewicz, P. Jurecka, Hobza, ChemPhysChem 6 (2005) 609.
[72] I.V. Alabugin, M. Manoharan, S. Peabody, F. Weinhold, J. Am. Chem. Soc. 125 (2003) 5973.
[73] J. Joseph, E.D. Jemmis, J. Am. Chem. Soc. 129 (2007) 4620.